oceans

MDPI

Article

An Experimental Approach to Assessing the Roles of Magnesium, Calcium, and Carbonate Ratios in Marine Carbonates

Claire E. Reymond * and Sönke Hohn

Leibniz Center for Tropical Marine Research (ZMT), Fahrenheitstr. 6, 28359 Bremen, Germany; soenke.hohn@googlemail.com

* Correspondence: claire.reymond@gmail.com

Abstract: Marine biomineralization is a globally important biological and geochemical process. Understanding the mechanisms controlling the precipitation of calcium carbonate [$CaCO_3$] within the calcifying fluid of marine organisms, such as corals, crustose coralline algae, and foraminifera, presents one of the most elusive, yet relevant areas of biomineralization research, due to the often-impenetrable ability to measure the process in situ. The precipitation of $CaCO_3$ is assumed to be largely controlled by the saturation state [Ω] of the extracellular calcifying fluid. In this study, we mimicked the typical pH and Ω known for the calcifying fluid in corals, while varying the magnesium, calcium, and carbonate concentrations in six chemo-static growth experiments, thereby mimicking various dissolved inorganic carbon concentration mechanisms and ionic movement into the extracellular calcifying fluid. Reduced mineralization and varied $CaCO_3$ morphologies highlight the inhibiting effect of magnesium regardless of pH and Ω and suggests the importance of strong magnesium removal or calcium concentration mechanisms. In respect to ocean acidification studies, this could allow an explanation for why specific marine calcifiers respond differently to lower saturation states.

Keywords: marine biomineralization; inorganic mineralization; coral reefs; ocean acidification (OA); omega; dissolved inorganic carbon (DIC); extracellular calcifying fluid (ECF)

Citation: Reymond, C.E.; Hohn, S. An Experimental Approach to Assessing the Roles of Magnesium, Calcium, and Carbonate Ratios in Marine Carbonates. *Oceans* **2021**, *2*, 193–214. https://doi.org/10.3390/oceans2010012

Academic Editor: Peter Schupp

Received: 30 August 2020
Accepted: 22 February 2021
Published: 3 March 2021

1. Introduction

Calcium carbonate ($CaCO_3$) is the most important biogenic mineral, in terms of quantity, global distribution, and diversity [1]. The production of $CaCO_3$ provides a number of ecological goods and services, such as shoreline protection and habitat structures. For example, coral reefs are one of the most important living bioconstructions of $CaCO_3$ [2] harboring one-quarter to one-third of all marine species [3], and thus serving to be socially and economically important [4]. Unfortunately, future projections show marine biomineralization will become severely impacted by ocean acidification (OA) due to the reduction of carbonate ion concentrations in the oceans [5,6].

Corals calcify extracellularly in a fluid that is separated from the seawater by at least two cell layers [7,8] and rely on a number of active and passive ionic exchanges. For example, calcium ions are actively transported into the extracellular calcifying fluid (ECF) by the epithelium cells of the coral polyp [9,10] while protons are removed [11], establishing favorable conditions for the precipitation of $CaCO_3$ [12]. Similarly, carbon either diffuses into the ECF as carbon dioxide [CO_2] or is actively transported into the ECF in the form of bicarbonate [13,14]. Some coral species can calcify in ocean water that is undersaturated with respect to aragonite [15], whereas other species cease to grow and vanish [16,17], which demonstrates a range of biological controls governing the mineralization process. Therefore, to understand which marine calcifiers will be affected by future reduction in ocean saturation states and to estimate its implications for the global carbon cycle, we need to explore a range of possible ECF scenarios.

The significance of biologically-induced and biologically-influenced mineralization is irrefutable. For example, the skeletal organic matrix [SOM] within corals is considered a major factor controlling the precipitation of $CaCO_3$. A number of studies have reported that the SOM contains not only acid-rich proteins (e.g., sulphated proteoglycans), but also assemblages of adhesion and structural proteins, which together are thought to provide a template for aragonite precipitation [10,18–20]. Additionally, the dissolution and precipitation of $CaCO_3$ in aqueous solution is largely dependent on abiotic factors relating to the saturation state (Ω) of the ECF [21,22], which is defined by the product of the dissolved ions forming the mineral divided by the stoichiometric solubility product, K_{sp}^* (Equation (1)).

$$\Omega = [Ca^{2+}]^*[CO_3^{2-}]/K_{sp}^*, \quad (1)$$

As expressed above, Ω is an extremely useful indicator of the equilibrium or disequilibrium of a solution with a mineral surface. When the ion product, $[Ca^{2+}]^*[CO_3^{2-}]$, equals the solubility product, K_{sp}^*, the saturation state equals one and the system is in equilibrium. If the saturation state is below one because the ion product is lower than the solubility product, the solution is undersaturated and the mineral dissolves. A saturation state higher than one indicates supersaturation where the product of the ion concentrations is greater than the solubility product. In this case, it is thermodynamically viable that dissolved ions precipitate into a crystal structure [22]. The observation that the precipitation rate of $CaCO_3$ increases with an increasing saturation state [21,23–27] has led to the development of empirical relationships (Equation (2)) that describe the calcification rate, G, as a function of the saturation state, where k is the reaction rate constant and n is the empirical reaction order.

$$G = k^*[\Omega - 1]^n, \quad (2)$$

This equation has been applied to predict calcification rates in corals [28] and has successfully been used to simulate the dynamics of ion concentrations in the calcifying fluid of corals and coccolithophores [14,28–30]. However, Equation (2) appears to ignore the theoretical basis shown in Figure 1, which emphasizes how the product of varying calcium and carbonate ion concentrations can obtain the same Ω value. This is also supported by [31], which demonstrated how the rate of calcite precipitation differed due to the ratio of calcium to carbonate despite having the same oversaturated Ω. Although Ω is a good predictor of dissolution and precipitation of $CaCO_3$, it does exclude the possibility that ion concentrations differ while obtaining the same Ω and could therefore account for observational variations among marine calcifiers.

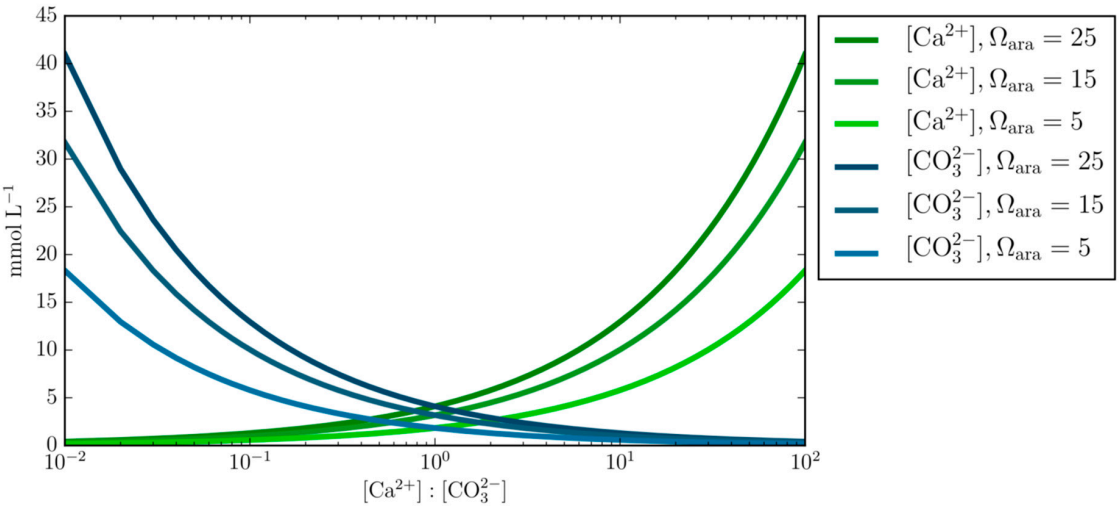

Figure 1. Varying concentrations of calcium and carbonate ions [Ca^{2+}:CO_3^{2-}] at fixed Ω_{ara} of 25, 15, and 5. This demonstrates the underlining principle that calcium and carbonate ion concentrations can obtain the same Ω_{ara} value at different Ca:CO_3 ratios, therefore questioning the empirical equation that prescribes the calcification rate as a function of Ω_{ara} alone.

Based on this rational, we decided to incubate coral skeleton fragments under six controlled abiotic chemo-static scenarios. By emulating previously measured ECF conditions, we kept all the solutions oversaturated in respect to Ω_{ara} = 10, pH 8.7, and maintained a typical tropical temperature of 25 °C. Experiment 1a recreated a magnesium [Mg] free condition (strong Mg removal activity) with a high $Ca:CO_3$ ratio (e.g., no dissolved inorganic carbon (DIC) concentrating mechanism and a weak proton removal from the ECF), while experiment 1b recreated a Mg-free solution with a low $Ca:CO_3$ ratio (e.g., mimicking a DIC concentrating mechanism resulting in DIC concentrations three times greater than ambient seawater and a strong proton removal from the ECF resulting in elevated total alkalinity ($_TA$) four times greater than ambient seawater). Experiment 2a recreated a medium Mg scenario (representing concentrations half that of the modern seawater) with a high $Ca:CO_3$ ratio, while experiment 2b recreated a medium Mg scenario with a low $Ca:CO_3$ ratio. Experiment 3a recreated a high Mg scenario (equal to that of modern seawater, i.e., no active removal of ions from the ECF) with a high $Ca:CO_3$ ratio, while experiment 3b recreated a high Mg scenario with a low $Ca:CO_3$ ratio.

2. Materials and Methods

2.1. Preparation of the Seed Material

There are a range of methodological approaches used to study $CaCO_3$ precipitation, previous studies have used powdered calcite 3–7 µm diameter as the seeding material [32], or Iceland spar [31], living specimens, e.g., [33,34], or synthetic crystals [35]. We used bioclastic fragments of *Stylophora pistillata* to add a potentially realistic coral aragonite crystal structure and investigate if active ion transport, as mediated by the coral calcifying tissue, suffices to drive coral calcification. The ion transporters of the tissue are simulated via the pumped fluids. Our experiment, therefore, aimed to mimic natural processes. However, the only biological component that was not included in the experiments were the organic molecules. This approach is also comparable to a recently published study that did include organic molecules in the incubations [36]. The seeding material for all experiments was obtained from aquarium grown *Stylophora pistillata* (Leibniz Center for Tropical Marine Research [ZMT], Bremen) and followed the methods of [36]. The coral skeleton fragments were cleaned for 48 h with hydrogen peroxide (H_2O_2 30%) to remove any soluble components and organic tissue. The coral skeleton fragments were then rinsed in Millipore® water, dried at 40 °C for 24 h, afterwards ground in a planetary ball mill (PM100, Retsch®) for 1 min, and dry sieved (1–200 µm). Individual bioclastic fragments were then hand-picked under a light microscope and selected based on uniform size and shape. These bioclasts are considered rough and represent a typical biogenic skeleton structure. The heterogenetic nature of coral skeletal structure adds a potentially realistic portrayal of the crystal surface adjustment to the ECF but also adds natural variability that occurs in all treatments. Afterwards, each bioclastic fragment was placed in an individual Eppendorf® Safe-Lock 0.5-mL microcentrifuge tube filled with ethanol and placed in an ultrasonic bath for 5 min to remove residual powder and again dried at 40 °C for 24 h. A by-product of this cleaning procedure could result in an increase of the micro-porosity of the bioclastic fragments, by the removal of organic material or breakage. Each fragment was weighed before and after the incubations on a Mettler Toledo® scale with a 1-µg precision (room humidity 30% and temperature 22 °C). As the size and weight of each bioclastic fragment was not perfectly uniform (0.364–1.449 g; Table A1), all bioclastic fragments were evenly distributed among treatments. The initial and end weights, and standardized daily weight increases can be found in the Appendix A (Table A1). To understand the difference in precipitation rate, a two-way factorial analysis of variance (ANOVA), least square (LS), and Tukey–Kramer honest significance difference (HSD) test of the standardized mean weight change between the six experimental scenarios were performed using the software JMP version 9.0. Microstructure formed during each experimental scenario was identified using a scanning electron microscope (Tescan Vega 3 XMU SEM, ZMT) back-scatter electron (BSE) images. Crystal structures of individual $CaCO_3$ polymorphs (vaterite, calcite and

aragonite) were analyzed under the Raman microscope at the Alfred Wegener Institute for Polar and Marine Research (AWI) in Bremerhaven, Germany, with the help of Dr. Gernot Nehrke. Due to the uneven surface of the incubated crystals, we did not perform a mapping of the whole crystal but focused on individual crystal structures to qualitatively identify the polymorphs with the Raman spectrum (Figure A1).

2.2. Experimental Setup

Ten custom-built incubation chambers made of Teflon [31,36] were used to conduct three cross-factor experiments with two Ca:CO_3 scenarios (high and low) in parallel with three Mg concentrations (0 mM, 26.5 mM, and 53 mM) in series (Figure 2; Table 1). Each chamber was attached with Tygon and Marprene® tubing to two 1-L Tedlar® gas sampling bags filled with either a calcium chloride [$CaCl_2$] or sodium bicarbonate [$NaHCO_3$], the preparation of the stock solution is detailed below. Five replicates were run for each treatment. The volume of each incubation chambers was 0.25 mL. The initial flow rate of the solutions into the chambers was accelerated to quickly fill the incubation chambers and then reduced to a constant flow (10 µL min^{-1}) via a 24-channel peristaltic pump (Ismatec®). The seed material was placed in each of the incubation chambers and the experiments were run between 32–70 days in a temperature-controlled Rumed® climate cabinet maintained at a constant 25 °C (±0.5 °C). The variation in experimental duration was due to unexpected health and safety issues of the authors not being allowed into the laboratory.

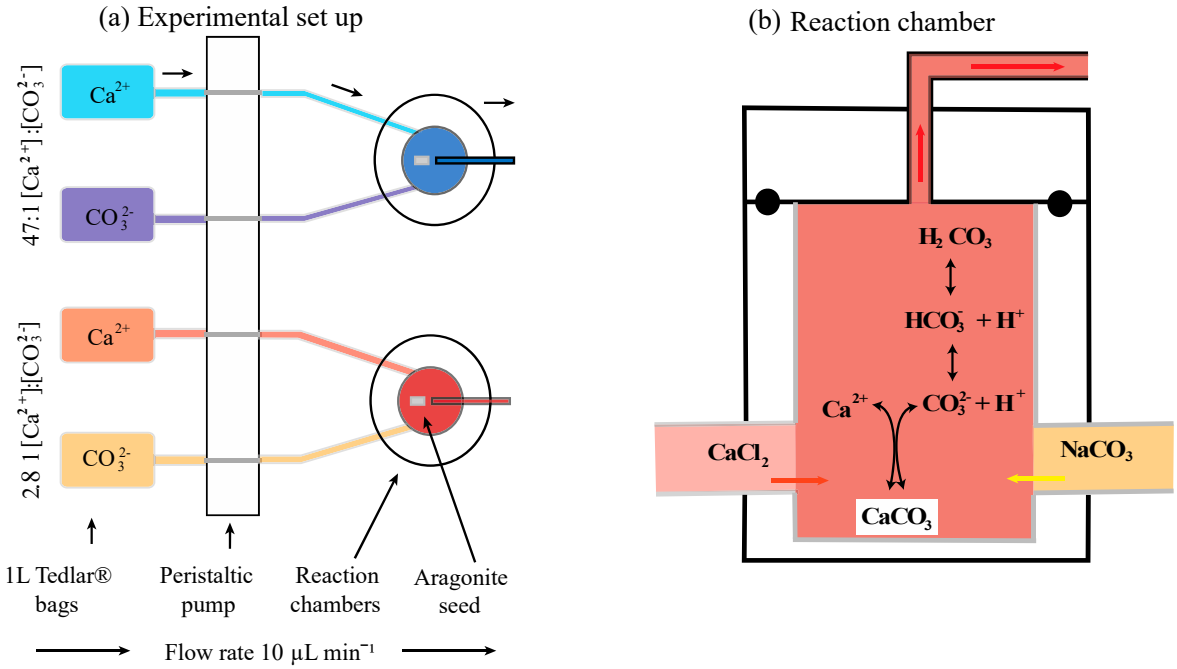

Figure 2. Schematic design of the experimental conditions showing (**a**) the separate stock solutions of Ca and CO_3 passing through the peristaltic pump and mixing in the reaction chambers, and (**b**) the physicochemical conversions of $CaCO_3$, bicarbonate [HCO_3^-] and CO_3 occurring during mineral precipitation and dissolution phases. Each of the six experimental scenarios is outlined in Table 1.

2.3. Preparation of Stock Solutions

All experiment stock solutions were prepared with Millipore® water, which was initially boiled to drive out dissolved CO_2 and then kept in a constant N_2 atmosphere to prevent CO_2 in-gassing. For all stock solutions pH was measured with a WTW-Multi 3430 Set K pH senor and calibrated with the pH 4 and 10 buffers at 25 °C. Among all the experiments temperature, salinity, and pH remained constant at 25 °C, 36, and 8.7, respectively. The aragonite saturation state, Ω_{ara} in all incubations was 10, with a satura-

tion index, $SI_{ara} = \log(\Omega_{ara})$, of 2.8, which should induce aragonite precipitation. These parameters represent conservative estimates of realistic scenarios for the coral ECF [11,37]. The aquatic properties chosen for the stock solutions in these experiments reflect the ECF parameters known for *Galaxea fascicularis*, but may not be representative for other coral species, e.g., [38,39]. The full details of the quantity of chemical compounds used for each experiment can be found in Table 2. Each chemical compound was weighed on a Mettler Toledo® scale with a 1µg precision (room humidity 30% and temperature 22 °C). Concentrations of $CaCl_2$ and magnesium chloride [$MgCl_2$] in the calcium stock solution and $NaHCO_3$ in the carbonate stock solution were double the target concentrations for calcium and carbonate ions because the fluids enter the incubation chambers at a 1:1 ratio and dilute each other's concentration by half (quantiles are given in Table 2A). After adding all the necessary chemical compounds to the stock solutions, they were transferred into 1-L Tedlar® gas sampling bags [36] and put into the climate cabinet at constant 25 °C (±0.5 °C). This study would improve greatly if microsensors were installed in the incubation chambers to monitor the real time chemistry. Unfortunately, our approach relies on the calculated parameters inside the chambers similar to the work of [31,36].

The calcium stock solutions were prepared by dissolving $CaCl_2$ in 5-L of carbon-free Millipore® water. For the experiments containing magnesium, $MgCl_2$ was added to the stock solution of $CaCl_2$. The Mg concentrations were chosen to represent a strong ion removal mechanism (0 mM, control Mg treatment), a medium ion removal mechanism [26.5 mM, equivalent to half the concentration in present day seawater], and a weak ion removal mechanism (53 mM, equivalent to the concentration in present day seawater). The amount of sodium chloride [NaCl] was then adjusted to maintain a final salinity of 36. Neither carbon nor alkalinity was present in the $CaCl_2$ stock solution (pH = 7), therefore maintaining a zero DIC and $_TA$ concentration.

The carbonate stock solutions were prepared by dissolving $NaHCO_3$ in 5-L of carbon-free Millipore® water. Sodium hydroxide [NaOH] was added via titration to adjust $_TA$ and to reach a pH of 8.716. The pH of the carbonate stock solution was 8.716 because when it mixes with the $CaCl_2$ solution (pH = 7) in the incubation chamber the pH will adjust to 8.700 because DIC and $_TA$ are known to mix conservatively [40]. DIC and $_TA$ were calculated for equilibrium carbonate chemistry in NaCl using the dissociation constants of [41].

Table 1. Solutions setup for incubation experiments. Calcium, magnesium, and DIC concentrations are arranged by the amounts of $CaCl_2$, $MgCl_2$, and $NaHCO_3$ added to the solutions. Temperature and salinity remained constant at 25 °C and 36 g kg^{-1}, respectively. Carbonate concentrations and $_TA$ are calculated for equilibrium carbonate chemistry in NaCl using the dissociation constants of [41].

Exp.	Ca^{2+}:CO_3^{2-}	Mg^{2+}:Ca^{2+}	Ca^{2+}	CO_3^{2-}	Mg^{2+}	Ω_{ara}	pH	DIC	$_TA$
	mol:mol	mol:mol	mM	µM	mM			µM	µM
1a	47	0	10.6	226	0	10	8.7	1777	2440
1b	2.8	0	2.6	926	0	10	8.7	7270	9885
2a	47	2.5	10.6	226	26.5	10	8.7	1777	2440
2b	2.8	10.2	2.6	926	26.5	10	8.7	7270	9885
3a	47	5	10.6	226	53	10	8.7	1777	2440
3b	2.8	20.4	2.6	926	53	10	8.7	7270	9885

Although the concentration of calcium in the ECF is known to vary, previous studies have recorded values between 9–15 mM from cold-water corals 9–12.3 mM with a mean of 9.9 mM; [42] and the tropical corals *Pocillopora damicornis* and *Acropora youngei* range between ca. 9–15 mM; [43]. The target value of 10.6 mM calcium, was chosen for the incubations with a high $Ca:CO_3$ (47:1) stoichiometry because it represents conditions measured with microelectrodes in the ECF of *Galaxea fascicularis* 9–11 mM; [11]. Although the target value of 2.6 mM calcium is perhaps unrealistically low, it was chosen for the incubations with a low $Ca:CO_3$ (2.8:1) stoichiometry to emulate a strong proton removal from the ECF (resulting in elevated $_TA$ four times greater than ambient seawater), as well

as a DIC concentrating mechanism (three times greater DIC than ambient seawater) as proposed by a number of authors [28,44–46]. These Ca:CO_3 stoichiometries were also chosen to maintain constant pH and Ω_{ara} between the treatments.

3. Results

3.1. Precipitation Rates

A highly significant interactive effect of Mg ion concentration and Ca:CO_3 concentration was observed (Figure 3; Table 2; $F_{[2,24]} = 150.924$, $p < 0.001$). When Mg was included into the aquatic solution, neither a significant weight change of the $CaCO_3$ seed nor a difference between the two Ca:CO_3 scenarios were observed (Table 2; Table A1). Conversely, both Mg-free Ca:CO_3 scenarios had significant weight increases. The Mg-free 47:1 Ca:CO_3 scenario had a calcification rate four times that of the Mg-free 2.8:1 Ca:CO_3 scenario (Figure 3, points labelled A and B). The average weight increase (± SD) in the Mg^-free 47:1 Ca:CO_3 treatment was 1.017 (± 0.130] mg d^{-1} and 0.229 (± 0.061) mg d^{-1} in the Mg-free 2.8:1 Ca:CO_3 treatment. The high amount of newly formed $CaCO_3$ measured in the Mg-free 47:1 Ca:CO_3^{2-} is partly explained by spontaneous nucleation, which was only observed in this scenario. Slight dissolution was observed under the intermediate (26.5 mM] and high (53 mM) Mg scenario with a 47:1 Ca:CO_3 concentration (−0.001 mg d^{-1} ± 0.001 and −0.002 mg d^{-1} ± 0.003, respectively). The intermediate and high Mg scenario with a 2.8:1 Ca:CO_3 concentration had no significant weight changes (0.000 mg d^{-1} ± 0.001 and 0.002 mg d^{-1} ± 0.007, respectively), the Ca:CO_3 concentration had no effect on the growth rate when Mg ion concentration was equal to or half that found in the ambient ocean, indicating that in this situation Mg has a stronger inhibiting effect towards calcification than Ca:CO_3 concentrations.

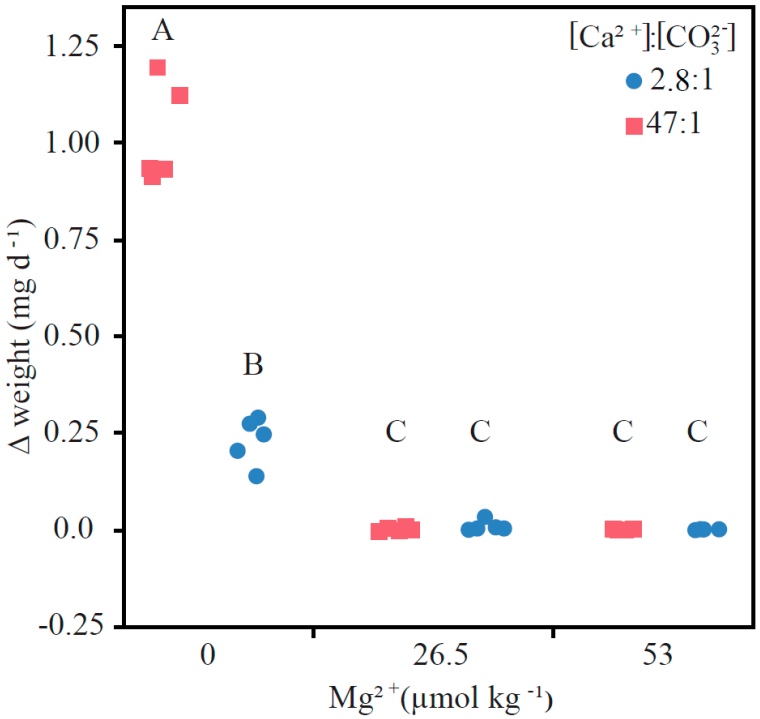

Figure 3. Scatter plot showing the standardized total weight change per day [mg d^{-1}] of each experimental scenario. The data shows a clear inhibiting effect of Mg and 2.8:1 Ca:CO_3 stoichiometry towards inorganic mineralization. Treatments not connected by the same alphabetical symbol (A, B, or C) are significantly different as shown in Table 2; $F_{[2,24]} = 150.924$, $p < 0.001$.

Table 2. Two-way factorial ANOVA and least square (LS) means difference. The effect test showed significant interaction between Ca:CO_3 and Mg concentration. Tukey–Kramer HSD comparisons indicates a significant difference between Mg-free and high Ca:CO_3, and all other treatments, as well as Mg-free and low Ca:CO_3 and all other treatments.

Source	DF	SS	MS	F-Ratio	$p > F$
Model	5	4.142	0.828	240.390	<0.001
Mg^{2+}	2	2.592		375.980	<0.001
Ca^{2+}:$CO_3{}^{2-}$	1	0.510		148.143	<0.001
Mg^{2+} * Ca^{2+}:$CO_3{}^{2-}$	2	1.040		150.924	<0.001
Error	24	0.083	0.003		
Total Error	29	4.224			

3.2. Mineralogy and Crystal Morphology

Back-scatter electron (BSE) images of the $CaCO_3$ surfaces show distinct morphological differences between the six treatments. The Mg-free (control Mg treatment) 47:1 Ca:CO_3 incubations formed homogeneous and heterogeneous nucleation in the form of crosshatched vaterite pre-spherical and laminated cubed calcite (Figure 4a). In the Mg-free 2.8:1 scenario, laminated cube calcite precipitated, along with amorphic calcium carbonate (ACC) or a stable prenucleation calcium carbonate cluster c.f. [47], and presumably unfinished calcite transforming from proto-vaterite precursors (Figure 4b). Despite the absence of a measurable weight increase from both the Mg addition scenarios with the 2.8:1 Ca:CO_3, newly formed aragonite needles were visibly precipitated on top of the seeding material (Figure 4d,f). Well-defined and abundant acicular crystals were precipitated in random directions and from multiple centers of nucleation as well as from cemented $CaCO_3$ (Figure 4f). In the scenario with high Mg concentration (equal to present day seawater, 53 mM) and at a 2.8:1 Ca:CO_3, $CaCO_3$, cements were also observed along with dissolution pits in a needle form (Figure 4f). In the scenario with lower Mg concentration (equal to half the present-day seawater, 26.5 mM) with a 47:1 Ca:CO_3, both ACC and dissolution pits were observed, in addition to Mg-calcite (Figure 4c). Conversely, in the scenario with the high Mg concentration and 47:1 Ca:CO_3, cements primarily formed along with dissolution pits, and low-relief aragonite needles within the seed material crevices (Figure 4e).

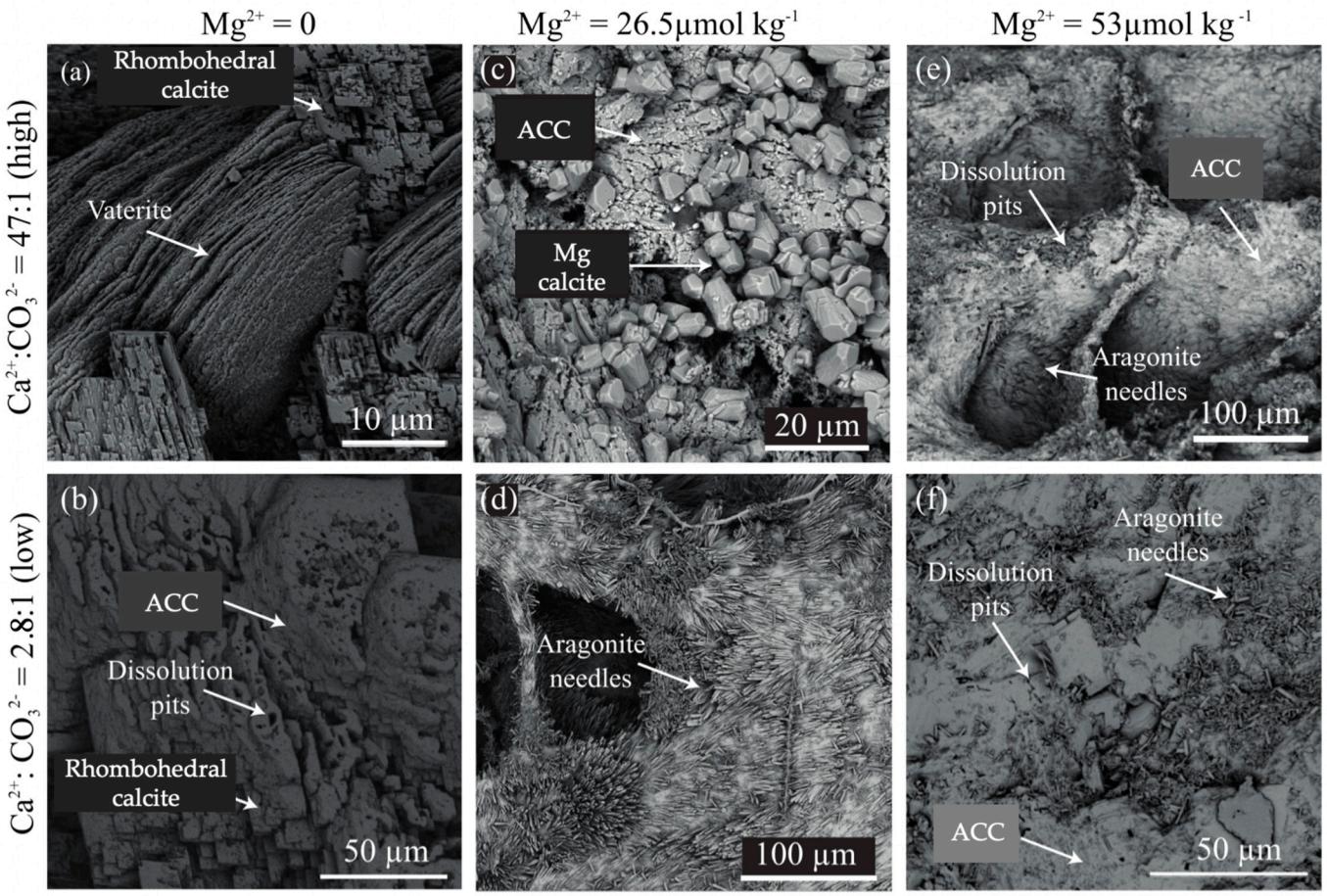

Figure 4. Representative SEM images of the precipitated $CaCO_3$ from each experimental scenario. This shows the influence of Ca:CO_3 stoichiometry, as well as the Mg concentration on the $CaCO_3$ morphology. The Mg-free incubations with a 47:1 Ca:CO_3 (**a**) resulted in crosshatched vaterite and layered rhombohedral calcite. Mg-free incubations (control Mg treamtent) with a 2.8:1 Ca:CO_3 stoichiometry (**b**) resulted in an intermediate form of ACC together with rhombohedral calcite and some signs of dissolution. Where the Mg concentration was half that of the modern seawater values (26.5 mM) and with a 47:1 Ca:CO_3 stoichiometry (**c**) resulted in a Mg-calcite structure c.f. [48]. Mg concentration of 26.5 mM with a 2.8:1 Ca:CO_3 stoichiometry (**d**) resulted in the formation of aragonite needles. In the scenario where the Mg concentration was 53 mM (equivalent to modern seawater values) no matter if the Ca:CO_3 stoichiometry was 2.8:1 or 47:1 (**e**,**f**) very little new $CaCO_3$ material precipitated, instead we can see ACC with low relief aragonite needles or unconnected aragonite needles and dissolution pits.

4. Discussion

This study compartmentalizes hypothetical abiotic conditions of the ECF, with the aim to gain a broader understanding of the chemical mechanisms relating to biomineralization among tropical marine calcifiers. We show that despite the same ion product of Ca and CO_3, calcification rates vary with different Ca:CO_3 ratios and Mg concentrations. In agreement with [31,36], this study emphasizes the importance of considering the ratio of Ca:CO_3 when estimating the Ω_{ara} within the ECF of marine calcifiers as exemplified in Figure 1. It is worth noting that in these experiments calcite and vaterite were also precipitated. The calculated Ω_{ara} in all experiments was 10, $\Omega_{calcite}$ was 15.15. Even though $\Omega_{vaterite}$ has been reported to be lower than Ω_{ara} and $\Omega_{calcite}$ it is not possible to calculate $\Omega_{vaterite}$ because this requires knowledge of the solubility product [49,50]. Our results show that high calcification rates, are not possible when the Mg concentration is equal to or half that of present-day oceanic concentrations, unless it is counterbalanced by a number of additional factors such as Ca:CO_3 stoichiometry, temperature, Ω_{ara}, proton pumping, or organic molecules. This study infers that the specific conditions required for $CaCO_3$ precipitation among marine

calcifiers is positively amplified by the organism. It is difficult to fully understand the process that controls biomineralization without further in situ ionic measurements from the ECF or more in vitro experiments.

4.1. Comparing Low and High Ca:CO_3 Scenarios

Generalized $CaCO_3$ precipitation models, as described by [23,28], present disagreement regarding the values for the coefficients n and k [24,25,51], which overestimate the calcification flux at low carbonate concentrations, e.g., when the ECF becomes DIC limited. It is well documented that biomineralization requires elevated Ω and in doing so implies DIC concentrating mechanisms [28,44–46]. However, direct DIC measurements from the ECF within tropical corals indicate concentrations similar to that of ambient seawater [37], which may result from high DIC consumption during calcification. As seen in previous studies, calcification among tropical corals can be maintained by elevating the Ca ions in the ECF to compensate decreasing seawater pH [43], while decreasing the strontium:calcium [Sr:Ca] and borate [$B(OH)_4$:CO_3^{2-}] ratios [52]. When comparing the low Ca:CO_3 (mimicking strong proton removal from the ECF resulting in elevated $_T$A four times greater than ambient seawater, and a DIC concentrating mechanism resulting in DIC three times greater than ambient seawater) with the high Ca:CO_3 scenario [ambient seawater DIC and $_T$A] at elevated pH = 8.7 and Ω_{ara} = 10 and 0 Mg [control Mg treatment], calcite precipitation rates were three times greater in the ambient seawater treatment than in the DIC concentrating mechanism treatment (Figure 3). This implies that ambient DIC is sufficient to induce calcification provided that homeostasis is maintained in the ECF and the DIC withdrawal from calcification is balanced by ionic flow rates in and out of the ECF [44–46].

4.2. The Connection between Mg and Calcification

Marine carbonate-producing organisms exert strong biogenic control to promote calcification within their ECF. This biogenic control is evident by the various mineralogy types and microstructures found among marine carbonate-producing organisms [53]. Calcite is preferentially precipitated as a function of lower temperatures and/or Mg:Ca ratios [54], in addition to the preferential substitution of Ca for Mg, e.g., high-Mg calcite [25]. For example, previous studies have shown coralline algae [33], scleractinian corals [34], and juvenile scleractinian coral [55] can produce calcite when the Mg:Ca ratio of seawater is <2 (e.g., Cretaceous calcitic seas) but at a slower rate. A recent study also found the presence of Mg ions to inhibit not only calcite nucleation during crystal formation but also aragonite [56]. Similarly, it has been shown that strontium also inhibits precipitation rates as a direct correlation with the aqueous calcium activity, thus preventing the attachment of calcium ions to the reactive sites [57,58]. Aragonite microstructure has also been shown to vary as a function of calcification rate, from rapidly formed granular centers of calcification to slower formed fibrous needles [59,60] as determined by the fractionation of $\delta^{18}O$ and $\delta^{13}C$ isotopes [61,62] and Mg:Ca ratios [59,60,63].

4.3. Polynucleation and Spontaneous Nucleation

The ratio of calcium to carbonate clearly matters within the ECF, as it has been shown to describe the rate and morphology of $CaCO_3$ (Figures 3 and 4). Precipitation pathways can be either direct or sequential depending on the free energy available on the surface as determined by pre-nucleation clusters (PNC), growth, and transformation [64–67]. Polynucleation occurred in all scenarios in this study, which led to a complex situation increasing the number of active sites on the surface layer, and therefore a stronger dependence on supersaturation than solely the layer-by-layer mineralization process [31]. Further complications arise because the rate-determining step may change with time as the number of defects and the relative dimensions of the crystal faces become modified during precipitation. Therefore, there are often deviations from the idealized kinetic models, as there may be a number of mechanisms operating in concert [66–68]. It is interesting to note

that spontaneous nucleation appeared in the experiment with high excess of calcium ions relative to carbonate ions (i.e., the ambient DIC and TA seawater treatment) but not in the low $Ca:CO_3$ treatment (i.e., the DIC concentrating mechanism scenario), however previous studies have shown that PNC usually form in a low $Ca:CO_3$ solution, equivalent to the binding of ions during crystal formation [47]. This may be due to metastable conditions under which precipitation of the mineral is delayed despite the solution being oversaturated in respect to Ω_{ara} [67].

The higher calcification rates in the Mg-free and 47:1 $Ca:CO_3$ scenario were obtained primarily due to spontaneous nucleation within the incubation chamber leading to much higher precipitation and thus greater reactive surface area. Previous calcite precipitation experiments in supersaturated ($\Omega_{calcite}$ 5, 16; pH = 10; T = 20 °C) conditions did not produce spontaneous nucleation and showed an optimum precipitation rate when $Ca:CO_3$ = 1:1 [31]. However, there are differences between this study and [31], one of which is the use of $NaHCO_3$ to prepare the carbonate solution in this study instead of K_2CO_3. This together with a temperature difference of 5 °C can potentially explain the variation between our observations and [31].

4.4. $CaCO_3$ Polymorphs

In the SEM images (Figure 4), the Mg-free high $Ca:CO_3$ scenario we see ACC, metastable inter-crosshatched vaterite pre-spheres, and rhombohedral calcite blocks. The sequential dissolution and re-precipitation mechanism can be explained via the kinetic rate, which is primarily controlled by the surface area of the crystal [69]. The mixture of vaterite and calcite suggests that calcite mineralization is the rate-determining step. The substitution of Mg into the ACC will however precipitate directly into calcite without the intermediate vaterite phase [70,71] as seen in the 2.5 Mg high $Ca:CO_3$ scenario (Figure 4c]. Under the present-day Mg:Ca ratio, aragonite dominates the kinetics of nucleation due to the calcite nucleation barrier being greater than metastable aragonite [72], which explains the lack of calcite in the high-Mg scenario. However, nucleation and precipitation in both the high-Mg scenarios where close to zero, implying that the aragonite seeding material was in equilibrium with the solution as shown by the dominance of ACC (Figure 4d–f) and dissolution pits in the shape of aragonite needles (Figure 4f).

The $Ca:CO_3$ ratio as well as the Mg concentration affected the $CaCO_3$ polymorph precipitated from the oversaturated solutions (Figure 4). In the Mg-free incubations, we obtained crosshatched vaterite and layered rhombohedral calcite in the high $Ca:CO_3$ scenario (Figure 4a] and an intermediate form of ACC together with rhombohedral calcite in the low $Ca:CO_3$ scenario (Figure 4b). In the incubations with 26.5 mM Mg, we obtained an unconnected Mg-calcite in the high $Ca:CO_3$ scenario (Figure 4c) and aragonite needles in the low $Ca:CO_3$ scenario (Figure 4d). With a 53 mM Mg concentration, representing normal seawater conditions, very little new material precipitated, most of which were ACC with sparse low relief aragonite needles (Figure 4e) or unconnected aragonite needles with dissolution pits in the form of needles (Figure 4f). Varying the $Ca:CO_3$, while keeping the Mg concentration fixed, changes the Mg:Ca ratio, which may have driven the differences in polymorphs shown in Figure 4c,d. Overall, the variety of polymorphs precipitated at a pH of 8.7 and an Ω_{ara} of 10 demonstrates that Ω alone does not control the precipitation process, as also suggested by [73]. Therefore, caution should be applied when inferring saturation state from the crystal morphology [60], particularly if other factors, e.g., Mg concentrations, temperature, or DIC, are not known.

Even though this study removes the organic aspect of biomineralization, organic molecules have been shown to act as a template to facilitate or induce crystallization [20,74–77] due to their strong binding potential with calcium ions [78,79]. The source of the organics is likely a combination of polyp-derived SOM and seawater-derived SOM as demonstrated from a comparison of coral skeletons and abiotic aragonite [80]. However, the presence of SOM or coral mucus in oversaturated solutions has also been shown to inhibit the nucleation of $CaCO_3$ [81] or pose no effect towards the rate of calcification [31]. Rather,

organic molecules appear to influence the $CaCO_3$ polymorph that precipitates from an oversaturated solution [31,77,82]. This suggests that organic molecules have a greater influence on the processes at the crystal surface that leads to the formation of a crystal structure, but not the kinetic processes, which transports the ions to the crystal surface.

An interesting observation from this study is that the aragonite needles precipitated in synthetic seawater (observed in the 26.5 mM Mg with a 2.8:1 $Ca:CO_3$ treatment] with no added biomolecules have a similar morphological appearance to synthetic aragonite experiments made from natural seawater, presumably with some residual organic carbon [60]. This could suggest that coral aragonite crystals may precipitate abiogenically after being initially nucleated, since abiotic systems that lack biomolecule templates altogether show similar morphologies.

4.5. Implications for Coral Reef Calcifiers

The concentrations of Mg or PO_4, which actively influence crystallization [21,23,24,67,83], are not well known for the ECF among marine organisms. Several studies assume the Mg concentrations in the ECF to be the same as in seawater and thus imply very high Ω_{ara} (>20) in order to explain the high precipitation rates as observed in corals [11,23,24,70–79,81,84]. Pioneer studies, which utilized various techniques, are largely in agreement with the range of Ω_{ara} in the ECF. For example, based on microsensor measurements, Ω_{ara} ranges from 11–25.5 [11,12,38,46], with the exception of 3.2 in the dark [11], 11–12.3 from Raman spectra [43,85], 11–25 inferred from $\delta^{11}B$ isotopes [44,86], 11.1–17.3 predicted by X-ray diffraction-based crystallographic estimates [87], and previously reviewed by [38] to range between 10.16–38.31. While, previous studies have reported the pH in the ECF to be 0.5–0.2 units higher than ambient seawater [46] and that homoeostasis can be maintained within the ECF regardless of varying external seawater pH [88]. Thus, implying a wide range of plausible $Ca:CO_3$ and Ca:Mg ratios within the ECF which enable $CaCO_3$ precipitation.

Measured Mg:Ca ratios from coral skeletons are between 1.5–5.5 mmol/mol [89–92] and from inorganic aragonite has between ~8.5–10 mmol/mol [59], while inorganic calcite has between 30–140 mmol/mol [93], demonstrating the importance of a Mg removal mechanism to facilitate the rate and morphology of calcification. Our results show that high calcification rates observed in corals are not possible when the Mg ion concentration in the ECF is equal to or half that of present day oceanic concentrations (Mg:Ca > 2.5). The high calcification rates observed in this study suggest a mechanism for active removal of inhibiting ions such as Mg from the coral ECF or a Ca concentration mechanism as suggested previously [43]. These points stress the well held belief that biomineralization is a highly complex and biologically mediated process, orchestrated by the secretion of organic molecules [94] and active ion transport [29].

Heterogeneous nucleation is largely inferred by the presence of biomolecules such as acid-rich proteins (e.g., sulphated proteoglycans) and various adhesion and structural proteins [10,18,19] are considered vital for the promotion and functioning of $CaCO_3$ structures. Additionally, the presence of SOM is known to influence the $CaCO_3$ crystal polymorph precipitated from over saturated solutions [82]. Recent experiments [36] confirmed an inhibiting role of coral organic molecules towards rate but not form of $CaCO_3$ [81]. For instance, the role of an ACC precursor phase is likely initiated by a series of controlled biomineralization mechanisms [95,96], particularly for polymorphic calcifying marine organisms. Heterogeneous nucleation has been observed in a range of marine calcifiers such as barnacles [97], echinoderms [95,98], coralline algae [99], foraminifera [100], and corals [43,96].

5. Conclusions

To understand the nuances of how coral reef calcifiers can adapt to global change, such as ocean acidification, we need to better understand the ionic composition at the site of calcification. Unfortunately, in the short-term tropical calcifying organisms show little acclimatization potential to ocean acidification [101] particularly when coupled with thermal

stress [102], but there are few examples of resistance by altering the ionic concentrations in the ECF, for example Ca [43]. Additionally, this study considered the influence of various $Ca:CO_3$ stoichiometry and Mg concentrations on the precipitation rates and morphology of $CaCO_3$ in a homeostatic experiment. Although there is still a need to conduct more experiments covering a range of other possible scenarios, we believe that our findings are highly relevant within the field of coral reef research for the following reasons:

1. Varying concentrations of calcium and carbonate ions at fixed Ω_{ara} demonstrates the underlining principal that calcium and carbonate ion concentrations can obtain the same Ω_{ara} value at different $Ca:CO_3$ stoichiometry and questions the generalized applicability of the empirical equation that prescribes the calcification rate as a function of Ω_{ara} alone.
2. As shown, calcifying fluid stoichiometry alters the precipitation rate and morphology of $CaCO_3$ at a constant Ω and pH. Therefore, our findings suggest caution should be applied when inferring saturation state from the crystal morphology, particularly if other factors e.g., Mg, temperature, or DIC are not known.
3. When comparing a strong proton removal scenario and a DIC concentrating mechanism to a scenario with ambient seawater pH and DIC conditions, calcite precipitation rates were three times greater in the ambient seawater conditions. Implying ambient seawater pH and DIC within the calcifying fluid is sufficient to induce calcification provided homeostasis is maintained.
4. Mg exerts a stronger effect on the instability of $CaCO_3$ than $Ca:CO_3$ stoichiometry, in which Mg incorporation locally disturbs the coordination environment in the aragonite structure [87,103]. These differences emphasize the importance of Mg removal from the calcifying fluid. Future studies are recommended to additionally monitor the Mg concentration in the calcifying fluid along with the carbon chemistry.

Author Contributions: C.E.R. and S.H., contributed equally to all aspects of this study from the conceptualization, methodology, validation, analysis, drafting, writing, and editing, visualization, project administration, and funding acquisition of this study. All authors have read and agreed to the published version of the manuscript.

Funding: This project was funded by the Leibniz Center for Tropical Marine Research [ZMT, Bremen] who is supported by the Ministerium für Kultur und Wissenschaft des Landes Nordrhein-Westfalen, the Regierende Bürgermeister von Berlin-inkl. Wissenschaft und Forschung, and the Bundesministerium für Bildung und Forschung.

Acknowledgments: Special thanks to Matthias Birkicht for analytical support and Gernot Nehrke for use of the CRM to identify the crystal polymorphs. We greatly appreciate the constructive comments from the three anonymous reviewers.

Conflicts of Interest: The authors declare no conflict of interest. The funders had no role in the design of the study; in the collection, analyses, or interpretation of data; in the writing of the manuscript, or in the decision to publish the results.

Appendix A

Table A1. Initial and final seed weights, including the duration of the experiment and the standardized weight change. Experimental identification corresponds to the aqueous conditions detailed in Table 1. The seed weight values are listed in grams, the experimental identification code is listed as Exp., the individual $CaCO_3$ bioclast identification is listed under Seed, the initial weight and end weight of the seed material correspond to column t_0 and t_e, the number of days in the experimental conditions is in column D (variation in experimental duration was due to unexpected health and safety issues), and the standardized weight change per day (g d^{-1}) is in column DΔ.

Exp.	Seed	t_0	t_e	D	DΔ
1a	1Mg-Free	0.480	30.290	32	0.932
1a	2Mg-Free	0.657	36.500	32	1.120
1a	3Mg-Free	0.883	30.620	32	0.929
1a	4Mg-Free	1.057	30.220	32	0.911
1a	5Mg-Free	1.202	39.370	32	1.193
1b	6Mg-Free	0.591	9.320	32	0.273
1b	7Mg-Free	0.862	5.260	32	0.137
1b	8Mg-Free	0.983	7.480	32	0.203
1b	9Mg-Free	1.064	10.300	32	0.289
1b	10Mg-Free	1.218	9.070	32	0.245
2a	1Mg	0.212	0.310	70	0.001
2a	2Mg	0.715	0.570	70	−0.002
2a	3Mg	0.777	0.649	70	−0.002
2a	4Mg	0.924	0.718	70	−0.003
2a	5Mg	1.013	1.006	70	0.000
2b	6Mg	0.423	0.322	70	−0.001
2b	7Mg	0.766	13.003	70	0.175
2b	8Mg	0.818	0.793	70	0.000
2b	9Mg	0.972	0.944	70	0.000
2b	10Mg	1.336	1.381	70	0.001
3a	1Mg +	0.364	0.360	38	0.000
3a	2Mg +	0.816	0.643	38	−0.005
3a	3Mg +	0.947	0.902	38	−0.001
3a	4Mg +	1.150	1.146	38	0.000
3a	5Mg +	1.274	1.212	38	−0.002
3b	6Mg +	0.668	0.534	38	−0.004
3b	7Mg +	0.918	0.922	38	0.000
3b	8Mg +	1.069	1.064	38	0.000
3b	9Mg +	1.220	1.237	38	0.000
3b	10Mg +	1.449	1.485	38	0.001

Table A2. The quantity of compounds (mg/5 L) added to the stock solution to obtain the experimental parameters outlined in Table 1.

Exp.	Calcium Stock (mg/5 L)			Carbonate Stock (mg/5 L)	
	$CaCl_2$	$MgCl_2$	NaCl	$NaHCO_3$	NaCl
1a	15.583	0.000	164.416	1.493	178.507
1b	3.809	0.000	176.191	6.107	173.893
2a	15.583	53.874	110.542	1.493	178.507
2b	3.809	53.874	122.316	6.107	173.893
3a	15.583	107.749	56.667	1.493	178.507
3b	3.809	107.749	68.442	6.107	173.893

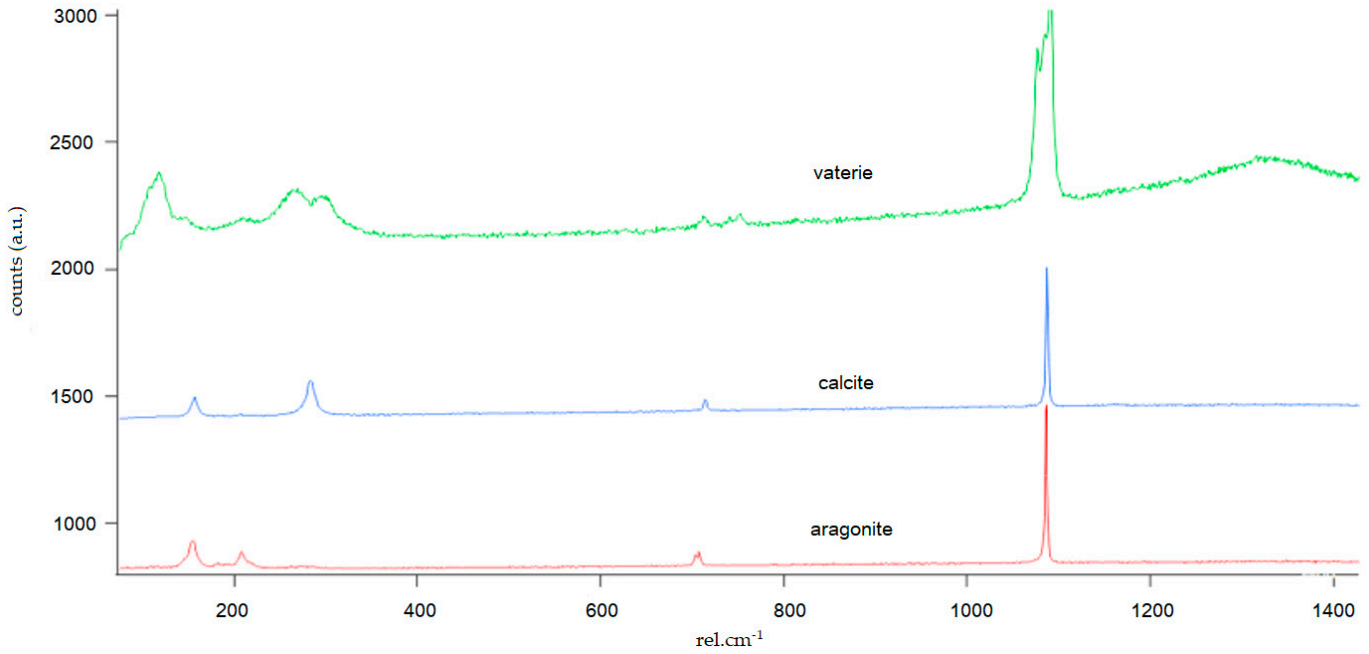

Figure A1. $CaCO_3$ polymorphs (aragonite, calcite, and vaterite) were identified via Raman spectroscopy, which were first morphologically identified by SEM on the incubated crystals. These Raman spectra were used to qualitatively identify the crystal structures found on the seeding crystals after incubation.

Script A1. Below are the calculations used to modify the artificial seawater for the six experiments.

```
# script for calculating salts and acids to set up solutions for experiment
import numpy as np
import scipy.optimize as opt
#*****************************************************************************************************
# some functions
def KstarW(tempK,salt): #after Millero_1995 p.670 Eq.63 and OA best practices guide
a0 = −1.384726e4
a1 = 1.489652e2
a2 = −2.36521e1
b0 = 1.1867e2
b1 = −5.977
b2 = 1.0495
g = −1.615e−2
lnKWT = a0/tempK + a1 + a2*np.log(tempK)
fT = b0/tempK + b1 + b2*np.log(tempK)
kstarw = np.exp(lnKWT + fT*(salt**0.5) + g*salt)
return kstarw
def Kstar1(tempK,salt): #after OA best practices guide
kstar1 = 10**(−3633.86/tempK + 61.2172−9.67770*np.log(tempK) + 0.011555*salt−0.0001152*salt**2.)
return kstar1
def Kstar2(tempK,salt): #after OA best practices guide
kstar2 = 10**(−471.78/tempK−25.9290 + 3.16967*np.log(tempK) + 0.01781*salt−0.0001122*salt**2.)
return kstar2
def Ksp_ara(tempK,salt):
ksp_ara = −171.945−0.077993*tempK + 2903.293/tempK + 71.595*np.log10(tempK) + (−0.068393 +0.0017276*tempK
+ 88.135/tempK)*salt**0.5−0.10018*salt + 0.0059415*salt**1.5 #mol2 kg−2
return 10.0**ksp_ara
def Kstar0(tempK,salt): # after Weiss, R. F., Marine Chemistry 2:203−215, 1974. (taken from CO2sys)
TempK100 = tempK/100.0;
```

```
    lnK0 = −60.2409 + 93.4517/TempK100 + 23.3585 * np.log(TempK100) + salt *(0.023517 - 0.023656 * TempK100 +
0.0047036 * TempK100 **2.)
    K0 = np.exp(lnK0) # this is in mol/kg-SW/atm
    return K0
    def Ksp_cal(tempK,salt):
    ksp_cal = −171.9065−0.077993*tempK + 2839.319/tempK + 71.595*np.log10(tempK) + (−0.77712 +0.0028426*tempK
+ 178.34/tempK)*salt**0.5−0.07711*salt + 0.0041249*salt**1.5 #mol2 kg−2
    return 10.0**ksp_cal
    #*********************************************************************************************************
    # molar masses
    m_Na = 22.98977 # [g/mol]
    m_Ca = 40.078 # [g/mol]
    m_Mg = 24.3050 # [g/mol]
    m_Cl = 35.4527 # [g/mol]
    m_C = 12.0107 # [g/mol]
    m_O = 15.9994 # [g/mol]
    m_H = 1.00794
    m_H2O= 2*m_H + m_O
    m_CaCl2 = m_Ca + 2.0*m_Cl + 2.0*m_H2O # [g/mol]
    m_MgCl2 = 203.30 # [g/mol]
    m_NaCl = m_Na + m_Cl # [g/mol]
    m_Na2CO3 = 2.0*m_Na + m_C + 3.0*m_O # [g/mol]
    m_NaHCO3 = m_Na + m_H + m_C + 3*m_O
    #*********************************************************************************************************
    # constant forcing and salt matrix
    Temperature = 25.0 # Celsius
    Salinity = 36.0 # we use g per kg
    TK = 273.15 + Temperature
    Sal = Salinity
    K0F = Kstar0(TK,Sal)
    K1F = Kstar1(TK,Sal)
    K2F = Kstar2(TK,Sal)
    KWF = KstarW(TK,Sal)
    Ksp = Ksp_ara(TK,Sal)
    Kspcal = Ksp_cal(TK,Sal)
    #*********************************************************************************************************
    #!!!!!!!!!!!!!!!!!!!!!!!!!!!!!!!!!!!!!!!!!!!!!!!!!!!!!!!!!!!!!!!!!!!!!!!!!!!!!!!!!!!!!!!!!!!!!!!!!!!!!!!!
    # input variables:
    # target values (in the experiment):
    pH_chamber = 8.7
    Omega_chamber = 10.0
    Mg_chamber = 53.0e−3/1.0 # mol kg−1
    #Ca_chamber = 10.60e−3 # mol kg−1
    # or
    Stoichiometry = 1.0/1.0 # mol Ca : mol CO3
    Ca_chamber = np.sqrt(Omega_chamber*Ksp*Stoichiometry)
    H_chamber = 10.0**(-pH_chamber)
    #!!!!!!!!!!!!!!!!!!!!!!!!!!!!!!!!!!!!!!!!!!!!!!!!!!!!!!!!!!!!!!!!!!!!!!!!!!!!!!!!!!!!!!!!!!!!!!!!!!!!!!!!
    #————————————————————————————————————————————-
    # calculated values
    # for the calculation of calcium and carbonate ions, I use two equations:
    # Stoichiometry = Calcium/CO3
    # Omega = Calcium*CO3/Ksp
    # # now I solve for CO3
```

```
# CO3 = Calcium/Stoichiometry
# CO3 = Omega*Ksp/Calcium
# Calcium/Stoichiometry = Omega*Ksp/Calcium # *Calcium *Stoichiometry
# Calcium**2 = Omega*Ksp*Stoichiometry
#————————————————————————————————————————————-
# once I know Calcium the rest is as follows
# (Chamber values)
CO3_chamber = Omega_chamber*Ksp/Ca_chamber # mol kg−1
DIC_chamber = CO3_chamber*(K1F*H_chamber + H_chamber*H_chamber + K1F*K2F)/(K1F*K2F)
CAlk_chamber = DIC_chamber*K1F*(H_chamber + 2.0*K2F)/(H_chamber*H_chamber + K1F*H_chamber + K1F*K2F)
OH_chamber = KWF/H_chamber
TA_chamber = CAlk_chamber + OH_chamber - H_chamber
Omegacal = Ca_chamber*CO3_chamber/Kspcal
print 'Omega calcite = ', Omegacal
#*****************************************************************************************************
# output
# (Chamber values)
print ' '
print 'expected values:'
print 'Ca =', Ca_chamber*1e3, 'e−3 mol kg-1'
print 'Mg =', Mg_chamber*1e3, 'e-3 mol kg-1'
print 'CO3 =', CO3_chamber*1e6, 'e-6 mol kg-1'
print 'pH =', pH_chamber
print 'DIC =', DIC_chamber*1e6, 'e-6 mol kg-1'
print 'TA =', TA_chamber*1e6, 'e-6 mol kg-1'
print 'Omega =', Omega_chamber
print 'stoichiometry =', Ca_chamber/CO3_chamber,': 1', '(mol Ca : mol CO3)'
print 'Cai paper: Omega=', 10.6e−3*600.0e−6/Ksp
#*****************************************************************************************************
# (Bag values)
print ' '
print 'the amounts of salts needed are:'
g_CaCl2 = Ca_chamber*m_CaCl2*2.0 # times two because the concentrations will be diluted in the chamber
g_MgCl2 = Mg_chamber*m_MgCl2*2.0 # times two because the concentrations will be diluted in the chamber
print g_CaCl2*5.0, 'g CaCl2 per 5 Liters'
print g_MgCl2*5.0, 'g MgCl2 per 5 Liters'
# (Bag values)
g_NaHCO3 = DIC_chamber*m_NaHCO3*2.0# times two because the concentrations will be diluted in the chamber
print g_NaHCO3*5.0, 'g NaHCO3 per 5 Liters'
print 'and to adjust salinity in the solutions we need:'
g_NaCl_1 = Salinity-g_CaCl2-g_MgCl2 # since Salinity is defined as g/kg
print g_NaCl_1*5.0, 'g NaCl per 5 Liters in the CaCl2 bag:'
g_NaCl_2 = Salinity-g_NaHCO3 # since Salinity is defined as g/kg
print g_NaCl_2*5.0, 'g NaCl per 5 Liters in the NaHCO3 bag:'
print 'remark:'
print '(Although I believe that the amount of carbonate might be overestimated and that measured Salinity might
actually be lower. However, we can test this with a calibrated salinity electrode.)'
#*****************************************************************************************************
print ' '
print ' '
print 'and the pH of the solutions will be:'
C0 = DIC_chamber*2.0
print 'DIC = ', C0
pKW = -np.log10(KWF)
```

```
pKS1 = -np.log10(K1F)
pKS2 = -np.log10(K2F)
pKB1 = pKW-pKS1
pKB2 = pKW-pKS2
print 'pKS1=', pKS1, 'pKS2=', pKS2
#pH_NaHCO3 = 0.5*(pKS1-np.log10(C0))
pH_NaHCO3 = pKW−0.5*(pKB1-np.log10(C0)) # this does not work because the approximation that the acid is only a 1 proton acid is too crude.
#pH_NaHCO3 = 0.5*(pKS1 + pKS2) # for an amphoter
print 'approximated pH for NaHCO3=', pH_NaHCO3
#*********************************************************************************************************
# now calculate the real pH
# molarity of base or acid to add
mol_base = 0.04 # mol L−1
mol_acid = 10.172/1000.0 # mol L−1
K0 = K0F
K1 = K1F
K2 = K2F
KW = KWF
# the function of the H+ concentration is an equation of fourth order and has to be solved numerically
# I use fmin to solve it:
# (Bag values)
DIC_CO3 = DIC_chamber*2.0
# the equation differs if you use NaHCO3 because the charge balance is slightly different:
def H_func_NaHCO3(H):
val = (KW/H + H*DIC_CO3/(H*H/(K2*K1) + H/K2 + 1.0)/K2 + 2.0*DIC_CO3/(H*H/(K2*K1) + H/K2 + 1.0)-H-DIC_CO3)**2.0
#print val
return val
# take a good guess from the approximation
H_init = 10**(-pH_NaHCO3)
H_opt = opt.fmin(H_func_NaHCO3, H_init, xtol = 0.1, ftol = 0.000001, maxiter = None, maxfun = None, full_output = 0, disp = 1, retall = 0, callback = None)
print 'print H for NaHCO3:'
print 'H for NaHCO3 = ', H_opt
pH_NaHCO3_opt = -np.log10(H_opt)
print 'print pH for NaHCO3:'
print 'the resulting pH of the NaHCO3 solution is', pH_NaHCO3_opt
#*********************************************************************************************************
# we will not adjust the pH of the CaCl2 bag !!!
# the milliQ is cooked and has a pH of 7
# adding CaCl2 does not add alkalinity, it might have a small effect on the pH due to CaOH and CaOH2
# we assume TA_Ca = 0.0; DIC_Ca = 0.0; and pH_Ca = 7.0
# (Bag values) Calcium Bag:
DIC_Ca = 0.0
TA_Ca =0.0
#*********************************************************************************************************
# now I have to calculate the required TA of the CO3 bag, which is double the TA in the chamber
TA_CO3 = TA_chamber*2.0
DIC_CO3 = DIC_chamber*2.0
print 'TA CO3=', TA_CO3*1e6
print 'DIC CO3=', DIC_CO3*1e6
# from this I have to derive the required pH of the solution
diff_TA = TA_CO3-DIC_CO3 # this is the amount of alkalinity that has to be added via NaOH
```

```
# so, basically, I have the amount of NaOH that has to be added (at least in theory)
print 'diff TA =', diff_TA*1e6
# (Bag values) Carbonate Bag:
#H_CO3 = 10.0**(-pH_target)
#OH_CO3 = KWF/H_CO3
#CAlk_CO3 = DIC_CO3*K1F*(H_CO3 + 2.0*K2F)/(H_CO3*H_CO3 + K1F*H_CO3 + K1F*K2F)
#TA_CO3 = CAlk_CO3 + OH_CO3 - H_CO3
#0 = DIC_CO3*K1F*(H_CO3 + 2.0*K2F)/(H_CO3*H_CO3 + K1F*H_CO3 + K1F*K2F) + KWF/H_CO3 - H_CO3 - TA_CO3
# the equation differs if you use NaHCO3 because the charge balance is slightly different:
def H_func_CO3bag(H):
val = (TA_CO3 - (DIC_CO3*K1F*(H + 2.0*K2F)/(H*H + K1F*H + K1F*K2F) + KWF/H - H))**2.0
#print val
return val
# take a good guess from the approximation
H_init = 10**(-pH_chamber)
H_opt = opt.fmin(H_func_CO3bag, H_init, xtol = 1e−12, ftol = 1e−12, maxiter=None, maxfun=None, full_output=0, disp=1, retall=0, callback=None)
print 'print target H for the NaHCO3 bag:'
print 'H for NaHCO3=', H_opt
pH_CO3_opt=-np.log10(H_opt)
print 'print target pH for the NaHCO3 bag:'
print 'the resulting pH of the NaHCO3 solution is', pH_CO3_opt
# test if this pH results the correct TA
CAlk_opt = DIC_CO3*K1F*(H_opt + 2.0*K2F)/(H_opt*H_opt + K1F*H_opt + K1F*K2F)
OH_opt = KWF/H_opt
TA_opt = CAlk_opt + OH_opt - H_opt
print 'TA CO3', TA_CO3*1e6, 'minus TA opt', TA_opt*1e6, '=', (TA_CO3-TA_opt)*1e6
#**********************************************************************************************************
# now titrate the NaHCO3 bag to the target pH
# and the same for the other solution
# (Bag values)
pH_start = 7.968 #pH_NaHCO3_opt
pH_target= pH_CO3_opt
#amount of acid needed (first calculated without buffering capacity)
mol_NaOH=10.0**(-pH_start)−10.0**(-pH_target)
# I have to calculate the amount of protons that are consumed also by the buffering system of the carbonate chemistry, and this on top of the pH change without the buffering capacity.
H_start=10.0**(-pH_start)
H_end=10.0**(-pH_target)
OH_start=KWF/H_start
OH_end=KWF/H_end
CO3_start=DIC_CO3*K1F*K2F/(K1F*H_start + H_start*H_start + K1F*K2F)
HCO3_start=DIC_CO3*K1F*H_start/(K1F*H_start + H_start*H_start + K1F*K2F)
H2CO3_start=DIC_CO3-HCO3_start-CO3_start
CO3_end=DIC_CO3*K1F*K2F/(K1F*H_end + H_end*H_end + K1F*K2F)
HCO3_end=DIC_CO3*K1F*H_end/(K1F*H_end + H_end*H_end + K1F*K2F)
H2CO3_end=DIC_CO3-HCO3_end-CO3_end
print 'CO3 from:', CO3_start*1e6, 'to', CO3_end*1e6, '\mu mol'
print 'HCO3 from:', HCO3_start*1e6, 'to', HCO3_end*1e6, '\mu mol'
print 'H2CO3 from:', H2CO3_start*1e6, 'to', H2CO3_end*1e6, '\mu mol'
H_diff=(2*H2CO3_start+HCO3_start+H_start-OH_start)-(2*H2CO3_end+HCO3_end+H_end-OH_end)
print 'mol NaOH needed to adjust pH_NaHCO3 from', pH_start, 'to', pH_target, 'is:', H_diff, 'compared to:', mol_NaOH, 'without considering the buffer capacity'
```

```
print 'at a molarity of ', mol_base, 'this requires ', H_diff/mol_base*1e3*5.0, 'ml of base for 5 L solution'
#*****************************************************************************************************
# added for review:
# calculate Omega calcite for comparison
Omegacal=Ca_chamber*CO3_chamber/Kspcal
print 'Omega calcite=', Omegacal
Omegaara=Ca_chamber*CO3_chamber/Ksp
print 'Omega aragonite=', Omegaara
```

References

1. Lowenstam, H.A.; Weiner, S. *On Biomineralization*; Oxford University Press: New York, NY, USA, 1989; p. 336.
2. Spalding, M.D.; Ravilious, C.; Green, E.P. *World Atlas of Coral Reefs*; University of California Press: Berkeley, CA, USA, 2001; p. 424.
3. Knowlton, N.; Brainard, R.E.; Fisher, R.; Moews, M.; Plaisance, L.; Caley, M.J. Coral Reef Biodiversity. In *Life in the World's Oceans: Diversity, Distribution, and Abundance*; Wiley online Books; McIntyre, A.D., Ed.; Blackwell Publishing Ltd.: Hoboken, NJ, USA, 2010; pp. 65–78.
4. Nystrom, M.; Folke, C.; Moberg, F. Coral reef disturbance and resilience in a human-dominated environment. *Trends Ecol. Evol.* **2000**, *15*, 413–417. [CrossRef]
5. Teng, H.H.; Dove, P.M.; Orme, C.A.; de Yoreo, J.J. Thermodynamics of calcite growth: Baseline for understanding biomineral formation. *Science* **1998**, *282*, 724–727. [CrossRef] [PubMed]
6. Hoegh-Guldberg, O.; Mumby, P.J.; Hooten, A.J.; Steneck, R.S.; Greenfield, P.; Gomez, E.; Harvell, C.D.; Sale, P.F.; Edwards, A.J.; Caldeira, K.; et al. Coral Reefs Under Rapid Climate Change and Ocean Acidification. *Science* **2007**, *318*, 1737–1742. [CrossRef] [PubMed]
7. Allemand, D.; Ferrierpages, C.; Furla, P.; Houlbreque, F.; Puverel, S.; Reynaud, S.; Tambutté, E.; Tambutté, S.; Zoccola, D. Biomineralisation in reef-building corals: From molecular mechanisms to environmental control. *Comptes Rendus Palevol.* **2004**, *3*, 453–467. [CrossRef]
8. Tambutté, S.; Holcomb, M.; Ferrier-Pagés, C.; Reynaud, S.; Tambutté, É.; Zoccola, D.; Allemand, D. Coral biomineralization: From the gene to the environment. *J. Exp. Mar. Bio Ecol.* **2011**, *408*, 58–78. [CrossRef]
9. Al-Horani, F.A.; Ferdelman, T.; Al-Moghrabi, S.M.; De Beer, D. Spatial distribution of calcification and photosynthesis in the scleractinian coral Galaxea fascicularis. *Coral. Reefs.* **2005**, *24*, 173–180. [CrossRef]
10. Tambutté, E.; Allemand, D.; Zoccola, D.; Meibom, A.; Lotto, S.; Caminiti, N.; Segonds, N. Observations of the tissue-skeleton interface in the scleractinian coral Stylophora pistillata. *Coral. Reefs.* **2007**, *26*, 517–529.
11. Al-Horani, F.A.; Al-Moghrabi, S.M.; De Beer, D. The mechanism of calcification and its relation to photosynthesis in the scleractinian coral *Galaxea fascicularis*. *Mar. Biol.* **2003**, *142*, 419–426. [CrossRef]
12. Ries, J.B. A physicochemical framework for interpreting the biological calcification response to CO_2 induced ocean acidification. *Geochim. Cosmochim. Acta.* **2011**, *75*, 4053–4064. [CrossRef]
13. Furla, P.; Allemand, D.; Orsenigo, M.N. Involvement of H^+ -ATPase and carbonic anhydrase in inorganic carbon uptake for endosymbiont photosynthesis. *Am. J. Physiol. Regul. Integr. Comp. Physiol.* **2000**, *278*, R870–R881. [CrossRef] [PubMed]
14. Hohn, S.; Merico, A. Modelling coral polyp calcification in relation to ocean acidification. *Biogeosciences* **2012**, *9*, 4441–4454. [CrossRef]
15. Venn, A.A.; Tambutté, E.; Holcomb, M.; Laurent, J.; Allemand, D.; Tambutté, S. Impact of seawater acidification on pH at the tissue–skeleton interface and calcification in reef corals. *Proc. Natl. Acad. Sci. USA* **2013**, *110*, 1634–1639. [CrossRef]
16. Fabricius, K.E.; De'ath, G.; Noonan, S.; Uthicke, S. Ecological effects of ocean acidification and habitat complexity on reef-associated macroinvertebrate communities. *Proc. R. Soc. B Biol. Sci.* **2014**, *81*, 2013479. [CrossRef]
17. Fabricius, K.E.; Langdon, C.; Uthicke, S.; Humphrey, C.; Noonan, S.; De 'ath, G.; Okazaki, R.; Muehllehner, N.; Glas, M.S.; Lough, J.M. Losers and winners in coral reefs acclimatized to elevated carbon dioxide concentrations. *Nat. Clim. Chang.* **2011**, *1*, 165–169. [CrossRef]
18. Muscatine, L.; Tambutte, E.; Allemand, D. Morphology of coral desmocytes, cells that anchor the calicoblastic epithelium to the skeleton. *Coral Reefs.* **1997**, *16*, 205–213. [CrossRef]
19. Mass, T.; Drake, J.L.; Peters, E.C.; Jiang, W.; Falkowski, P.G. Immunolocalization of skeletal matrix proteins in tissue and mineral of the coral *Stylophora pistillata*. *Proc. Natl. Acad. Sci. USA* **2014**, *111*, 12728–12733. [CrossRef]
20. Cuif, J.-P.; Dauphin, Y. The Environment Recording Unit in coral skeletons—a synthesis of structural and chemical evidences for a biochemically driven, stepping-growth process in fibres. *Biogeosciences* **2005**, *2*, 61–73. [CrossRef]
21. Lippmann, F. *Sedimentary Carbonate Minerals*; Springer: Berlin/Heidelberg, Germany, 1973; p. 228.
22. Lasaga, A.C. *Kinetic Theory in the Earth Sciences*; Princeton University Press: Princeton, NJ, USA, 2014; p. 822.
23. Burton, E.A.; Walter, L.M. Relative precipitation rates of aragonite and Mg calcite from seawater: Temperature or carbonate ion control? *Geology* **1987**, *15*, 111–114. [CrossRef]
24. Burton, E.A.; Walter, L.M. The role of pH in phosphate inhibition of calcite and aragonite precipitation rates in seawater. *Geochim. Cosmochim. Acta* **1990**, *54*, 797–808. [CrossRef]

25. Zuddas, P.; Mucci, A. Kinetics of calcite precipitation from seawater: I. A classical chemical kinetics description for strong electrolyte solutions. *Geochim. Cosmochim. Acta* **1994**, *58*, 4353–4362. [CrossRef]
26. Reddy, M.M.; Nancollas, G.H. The crystallization of calcium carbonate. *IV. The effect of magnesium, strontium and sulfate ions. J. Cryst. Growth* **1976**, *35*, 33–38. [CrossRef]
27. Gattuso, J.P.; Frankignoulle, M.; Bourge, I.; Romaine, S.; Buddemeier, R.W. Effect of calcium carbonate saturation of seawater on coral calcification. *Glob. Planet Chang.* **1998**, *18*, 37–46. [CrossRef]
28. McCulloch, M.; Falter, J.; Trotter, J.; Montagna, P. Coral resilience to ocean acidification and global warming through pH up-regulation. *Nat. Clim. Chang.* **2012**, *2*, 623–627. [CrossRef]
29. Hohn, S.; Merico, A. Quantifying the relative importance of transcellular and paracellular ion transports to coral polyp calcification. *Front Earth Sci.* **2015**, *2*, 1–11. [CrossRef]
30. Holtz, L.M.; Wolf-Gladrow, D.; Thoms, S. Simulating the effects of light intensity and carbonate system composition on particulate organic and inorganic carbon production in Emiliania huxleyi. *J. Theor. Biol.* **2015**, *372*, 192–204. [CrossRef]
31. Nehrke, G.; Reichart, G.J.; Van Cappellen, P.; Meile, C.; Bijma, J. Dependence of calcite growth rate and Sr partitioning on solution stoichiometry: Non-Kossel crystal growth. *Geochim. Cosmochim. Acta* **2007**, *71*, 2240–2249. [CrossRef]
32. Hartley, G.; Mucci, A. The influence of P_{CO2} on the partitioning of magnesium in calcite overgrowth precipitated from artificial seawater at 25° and 1 atm total pressure. *Geochim. Cosmochim. Acta* **1996**, *60*, 315–324. [CrossRef]
33. Ries, J.B. Aragonitic Algae in Calcite Seas: Effect of Seawater Mg/Ca Ratio on Algal Sediment Production. *J. Sediment Res.* **2006**, *76*, 515–523. [CrossRef]
34. Ries, J.B.; Stanley, S.M.; Hardie, L.A. Scleractinian corals produce calcite, and grow more slowly, in artificial Cretaceous seawater. *Geology* **2006**, *34*, 525–528. [CrossRef]
35. Kim, Y.-Y.; Ganesan, K.; Yang, P.; Kulak, A.N.; Borukhin, S.; Pechook, S.; Ribeiro, L.; Kröger, R.; Eichhorn, S.J.; Armes, S.P.; et al. An artificial biomineral formed by incorporation of copolymer micelles in calcite crystals. *Nat. Mater.* **2011**, *10*, 890–896. [CrossRef] [PubMed]
36. Hohn, S.; Reymond, C.E. Coral calcification, mucus, and the origin of skeletal organic molecules. *Coral Reefs.* **2019**, *38*, 973–984. [CrossRef]
37. Cai, W.-J.; Ma, Y.; Hopkinson, B.M.; Grottoli, A.G.; Warner, M.E.; Ding, Q.; Hu, X.; Yuan, X.; Schoepf, V.; Xu, H.; et al. Microelectrode characterization of coral daytime interior pH and carbonate chemistry. *Nat. Commun.* **2016**, *4*, 11144. [CrossRef]
38. Raybaud, V.; Tambutté, S.; Ferrier-Pagès, C.; Reynaud, S.; Venn, A.A.; Tambutté, É.; Nival, P.; Allemand, D. Computing the carbonate chemistry of the coral calcifying medium and its response to ocean acidification. *J. Theor. Biol.* **2017**, *424*, 26–36. [CrossRef] [PubMed]
39. Sevilgen, D.S.; Venn, A.A.; Hu, M.Y.; Tambutté, E.; de Beer, D.; Planas-Bielsa, V.; Tambutté, S. Full in vivo characterization of carbonate chemistry at the site of calcification in corals. *Sci. Adv.* **2019**, *5*, 7447. [CrossRef] [PubMed]
40. Wolf-Gladrow, D.A.; Zeebe, R.E.; Klaas, C.; Körtzinger, A.; Dickson, A.G. Total alkalinity: The explicit conservative expression and its application to biogeochemical processes. *Mar. Chem.* **2007**, *106*, 287–300. [CrossRef]
41. Millero, F.; Huang, F.; Graham, T.; Pierrot, D. The dissociation of carbonic acid in NaCl solutions as a function of concentration and temperature. *Geochim. Cosmochim. Acta* **2007**, *71*, 46–55. [CrossRef]
42. Schleinkofer, N.; Raddatz, J.; Freiwald, A.; David Evans, D.; Beuck, L.; Rüggeberg, A.; Liebetrau, V. Environmental and biological controls on Na/Ca ratios in scleractinian cold-water corals. *Biogeosciences* **2019**, *16*, 3565–3582. [CrossRef]
43. DeCarlo, T.M.; Comeau, S.; Cornwall, C.E.; McCulloch, M.T. Coral resistance to ocean acidification linked to increased calcium at the site of calcification. *Proc. R. Soc. B Biol. Sci.* **2018**, *285*, 1878. [CrossRef] [PubMed]
44. Allison, N.; Cohen, I.; Finch, A.A.; Erez, J.; Tudhope, A.W. Corals concentrate dissolved inorganic carbon to facilitate calcification. *Nat. Commun.* **2014**, *5*, 5741. [CrossRef] [PubMed]
45. de Nooijer, L.J.; Spero, H.J.; Erez, J.; Bijma, J.; Reichart, G.J. Biomineralization in perforate Foraminifera. *Earth Sci. Rev.* **2014**, *135*, 48–58. [CrossRef]
46. Venn, A.A.; Tambutté, E.; Holcomb, M.; Allemand, D.; Tambutté, S. Live tissue imaging shows reef corals elevate pH under their calcifying tissue relative to seawater. *PLoS ONE* **2011**, *6*, e20013.65. [CrossRef]
47. Gebauer, D.; Völkel, A.; Cölfen, H. Stable prenucleation calcium carbonate clusters. *Science* **2009**, *322*, 1819–1822. [CrossRef] [PubMed]
48. Ihli, J.; Clark, J.N.; Kanwal, N.; Kim, Y.-Y.; Holden, M.A.; Harder, R.J.; Tang, C.C.; Ashbrook, S.E.; Robinson, I.K.; Meldrum, F.C. Visualization of the effect of additives on the nanostructures of individual bio-inspired calcite crystals. *Chem. Sci.* **2019**, *10*, 1176–1185. [CrossRef]
49. Plummer, L.N.; Busenberg, E. The solubilities of calcite, aragonite and vaterite in CO2-H2O solutions between 0 and 90 °C, and an evaluation of the aqueous model for the system CaCO3-CO2-H2O. *Geochim. Cosmochim. Acta* **1982**, *46*, 1011–1040. [CrossRef]
50. De Visscher, A.; Vanderdeelen, J. Estimation of the Solubility Constant of Calcite, Aragonite, and Vaterite at 25°C Based on Primary Data Using the Pitzer Ion Interaction Approach. *Monatshefte fur Chemie* **2003**, *134*, 769–775. [CrossRef]
51. Zhong, S.; Mucci, A. Calcite precipitation in seawater using a constant addition technique: A new overall reaction kinetic expression. *Geochim. Cosmochim. Acta* **1993**, *57*, 1409–1417.
52. Allison, N.; Finch, A.A. δ11B, Sr, Mg and B in a modern Porites coral: The relationship between calcification site pH and skeletal chemistry. *Geochim. Cosmochim. Acta* **2010**, *74*, 1790–1800. [CrossRef]

53. Opdyke, B.N.; Wilkinson, B.H. Paleolatitude distribution of Phanerozoic marine ooids and cements. *Palaeogeogr Palaeoclim Palaeoecol* **1990**, *78*, 135–148. [CrossRef]
54. Morse, J.W.; Wang, Q.; Tsio, M.Y. Influences of temperature and Mg: Ca ratio on $CaCO_3$ precipitates from seawater. *Geology* **1997**, *25*, 85–87. [CrossRef]
55. Higuchi, T.; Fujimura, H.; Yuyama, I.; Harii, S.; Agostini, S.; Oomori, T. Biotic control of skeletal growth by scleractinian corals in aragonite–calcite seas. *PLoS ONE* **2014**, *9*, e91021. [CrossRef]
56. Boon, M.; Rickard, W.D.; Rohl, A.L.; Jones, F. Stabilization of Aragonite: Role of Mg^{2+} and Other Impurity Ions. *Cryst. Growth Des.* **2020**, *20*, 5006–5017. [CrossRef]
57. Bracco, J.N.; Grantham, M.C.; Stack, A.G. Calcite Growth Rates as a Function of Aqueous Calcium-to-Carbonate Ratio, Saturation Index, and Inhibitor Concentration: Insight into the Mechanism of Reaction and Poisoning by Strontium. *Cryst. Growth Des.* **2012**, *12*, 3540–3548. [CrossRef]
58. Gebrehiwet, T.A.; Redden, G.D.; Fujita, Y.; Beig, M.S.; Smith, R.W. The Effect of the CO_3^{2-} to Ca^{2+} Ion activity ratio on calcite precipitation kinetics and Sr^{2+} partitioning. *Geochem. Trans.* **2012**, *13*, 1–11. [CrossRef]
59. Gaetani, G.A.; Cohen, A.L. Element partitioning during precipitation of aragonite from seawater: A framework for understanding paleoproxies. *Geochim. Cosmochim. Acta* **2006**, *70*, 4617–4634. [CrossRef]
60. Holcomb, M.; Cohen, A.L.; Gabitov, R.; Hutter, J. Compositional and morphological features of aragonite precipitated experimentally from seawater and biogenically by corals. *Geochim. Cosmochim. Acta* **2009**, *73*, 166–179. [CrossRef]
61. Adkins, J.F.; Boyle, E.A.; Curry, W.B.; Lutringer, A. Stable isotopes in deep-sea corals and a new mechanism for "vital effects". *Geochim. Cosmochim. Acta* **2003**, *67*, 1129–1143. [CrossRef]
62. Rollion-Bard, C.; Chaussidon, M.; France-Lanord, C. pH control on oxygen isotopic composition of symbiotic corals. *Earth Planet Sci. Lett.* **2003**, *215*, 275–288. [CrossRef]
63. Watson, E.B. A conceptual model for near-surface kinetic controls on the trace- element and stable isotope composition of abiogenic calcite crystals. *Geochim. Cosmochim. Acta* **2004**, *68*, 1473–1488. [CrossRef]
64. Boistelle, R.; Astier, J.P. Crystallization mechanisms in solution. *J. Cryst. Growth.* **1988**, *90*, 14–30. [CrossRef]
65. Davey, R.J.; Schroeder, S.L.M.; Ter Horst, J.H. Nucleation of organic crystals—A molecular perspective. *Angew Chemie Int. Ed.* **2013**, *52*, 2167–2179. [CrossRef]
66. Mann, S. *Biomineralization: Principles and Concepts in Bioinorganic Materials Chemistry*; Oxford University Press: Oxford, UK, 2001; p. 210.
67. Gebauer, D.; Kellermeier, M.; Gale, J.D.; Bergström, L.; Cölfen, H. Pre-nucleation clusters as solute precursors in crystallisation. *Chem. Soc. Rev.* **2014**, *43*, 2348–2371. [CrossRef]
68. Bonucci, E. Role of collagen fibrils in calcification. In *Calcification in Biological Systems*; Bonucci, E., Ed.; CRC Press: Boca Raton, FL, USA, 1992; pp. 19–39.
69. Rodriguez-Blanco, J.D.; Shaw, S.; Benning, L.G. The kinetics and mechanisms of amorphous calcium carbonate [ACC] crystallization to calcite, viavaterite. *Nanoscale* **2011**, *3*, 265–271. [CrossRef] [PubMed]
70. Wray, J.; Daniels, F. Precipitation of calcite and aragonite. *J. Am. Chem. Soc.* **1957**, *79*, 2031–2034. [CrossRef]
71. Ogino, T.; Suzuki, T.; Sawada, K. The formation and transformation mechanism of calcium carbonate in water. *Geochemica Cosmochem Acta.* **1987**, *51*, 2757–2767. [CrossRef]
72. Sun, W.; Jayaraman, S.; Chen, W.; Persson, K.A.; Ceder, G. Nucleation of metastable aragonite CaCO3 in seawater. *Proc Natl. Acad. Sci. USA* **2015**, *112*, 3199–3204. [CrossRef]
73. Cyronak, T.; Schulz, K.G.; Jokiel, P.L. The Omega myth: What really drives lower calcification rates in an acidifying ocean. *ICES J. Mar. Sci.* **2016**, *73*, 558–562. [CrossRef]
74. Allemand, D.; Tambutte, E.; Girard, J.; Jaubert, J.; Tambutté, E.; Girard, J.; Jaubert, J. Organic matrix synthesis in the scleractinian coral Stylophora pistillata: Role in biomineralization and poten- tial target of the organotin tributyltin. *J. Exp. Biol.* **1998**, *201*, 2001–2009. [PubMed]
75. Watanabe, T.; Fukuda, I.; China, K.; Isa, Y. Molecular analyses of protein components of the organic matrix in the exoskeleton of two scleractinian coral species. *Comp. Biochem. Physiol. B Biochem. Mol. Biol.* **2003**, *136*, 767–774. [CrossRef]
76. Helman, Y.; Natale, F.; Sherrell, R.M.; LaVigne, M.; Starovoytov, V.; Gorbunov, M.Y.; Falkowski, P.G. Extracellular matrix production and calcium carbonate precipitation by coral cells in vitro. *Proc. Natl. Acad. Sci. USA* **2008**, *105*, 54–58. [CrossRef] [PubMed]
77. Mass, T.; Drake, J.L.; Haramaty, L.; Kim, J.D.; Zelzion, E.; Bhattacharya, D.; Falkowski, P.G. Cloning and characterization of four novel coral acid-rich proteins that precipitate carbonates *in vitro*. *Curr. Biol.* **2003**, *23*, 1126–1131. [CrossRef]
78. Kretsinger, R.H. Calcium-Binding Proteins. *Ann. Rev. Biochem.* **1976**, *45*, 239–266. [CrossRef] [PubMed]
79. Carafoli, E. Intracellular Calcium Homeostasis. *Ann. Rev. Biochem.* **1987**, *56*, 395–433. [CrossRef]
80. DeCarlo, T.M.; Ren, H.; Farfan, G.A. The Origin and Role of Organic Matrix in Coral Calcification: Insights from Comparing Coral Skeleton and Abiogenic Aragonite. *Front Mar. Sci.* **2018**, *5*, 170. [CrossRef]
81. Marin, F.; Smith, M.; Isa, Y.; Muyzer, G.; Westbroek, P. Skeletal matrices, muci, and the origin of invertebrate calcification. *Proc. Natl. Acad. Sci. USA* **1996**, *93*, 1554–1559. [CrossRef]
82. Westbroek, P.; Marin, F. A marriage of bone and nacre. *Nature* **1998**, *392*, 861–862. [CrossRef] [PubMed]

83. Kawano, J.; Sakuma, H.; Nagai, T. Incorporation of Mg^{2+} in surface Ca^{2+} sites of aragonite: An ab initio study. *Prog. Earth Planet Sci.* **2015**, *2*, 7. [CrossRef]
84. Cohen, A.L.; McConnaughey, T.A. Geochemical Perspectives on Coral Mineralization. *Rev. Mineral. Geochem.* **1990**, *4*, 151–187.
85. DeCarlo, T.M.; D'Olivo, J.P.; Foster, T.; Holcomb, M.; Becker, T.; McCulloch, M.T. Coral calcifying fluid aragonite saturation states derived from Raman spectroscopy. *Biogeosciences* **2017**, *14*, 5253–5269. [CrossRef]
86. McCulloch, M.; Trotter, J.; Montagna, P.; Falter, J.; Dunbar, R.; Freiwald, A.; Försterra, G.; López Correa, M.; Maier, C.; Rüggeberg, A.; et al. Resilience of cold-water scleractinian corals to ocean acidification: Boron isotopic systematics of pH and saturation state up-regulation. *Geochim. Cosmochim. Acta.* **2012**, *87*, 21–34. [CrossRef]
87. Farfan, G.A.; Cordes, E.E.; Waller, R.G.; DeCarlo, T.M.; Hansel, C.M. Mineralogy of Deep-Sea Coral Aragonites as a Function of Aragonite Saturation State. *Front. Mar. Sci.* **2018**, *5*, 473. [CrossRef]
88. Georgiou, L.; Falter, J.; Trotter, J.; Kline, D.I.; Holcomb, M.; Dove, S.G.; Hoegh-Guldberg, O.; Mcculloch, M. pH homeostasis during coral calcification in a free ocean CO_2 enrichment [FOCE] experiment, Heron Island reef flat, Great Barrier Reef. *Proc. Natl. Acad. Sci. USA* **2015**, *112*, 13219–13224. [CrossRef]
89. Mitsuguchi, T.; Matsumoto, E.; Abe, O.; Uchida, T.; Isdale, P.J. Mg/Ca Thermometry in Coral Skeletons. *Science.* **1996**, *274*, 961–963. [CrossRef] [PubMed]
90. Gaetani, G.A.; Cohen, A.L.; Wang, Z.; Crusius, J. A biomineralization approach to developing climate proxies. *Geochim. Cosmochim. Acta* **2011**, *75*, 1920–1932. [CrossRef]
91. Wei, G.; Sun, M.; Li, X.; Nie, B. Mg/Ca, Sr/Ca and U/Ca ratios of a porites coral from Sanya Bay, Hainan Island, South China Sea and their relationships to sea surface temperature. *Palaeogeogr Palaeoclimatol Palaeoecol.* **2000**, *162*, 59–74. [CrossRef]
92. Marchitto, T.M.; Bryan, S.P.; Doss, W.; McCulloch, M.T.; Montagna, P. A simple biomineralization model to explain Li, Mg, and Sr incorporation into aragonitic foraminifera and corals. *Earth Planet Sci. Lett.* **2018**, *481*, 20–29. [CrossRef]
93. De Choudens-Sánchez, V.; González, L.A. Calcite and aragonite precipitation under controlled instantaneous supersaturation: Elucidating the role of CaCO3 saturation state and Mg/Ca ratio on calcium carbonate polymorphism. *J. Sediment. Res.* **2009**, *79*, 363–376. [CrossRef]
94. Falini, G.; Fermani, S.; Goffredo, S. Seminars in Cell & Developmental Biology Coral biomineralization: A focus on intra-skeletal organic matrix and calcification. *Semin. Cell Dev. Biol.* **2015**, *46*, 17–26. [PubMed]
95. Politi, Y.; Arad, T.; Klein, E.; Weiner, S.; Addadi, L. Sea urchin spine calcite forms via a transient amorphous calcium carbonate phase. *Science* **2004**, *306*, 1161–1164. [CrossRef]
96. Mass, T.; Giuffre, A.J.; Sun, C.-Y.; Stifler, C.A.; Frazier, M.J.; Neder, M.; Tamura, N.; Stan, C.V.; Marcus, M.A.; Gilbert, P.U.P.A. Amorphous calcium carbonate particles form coral skeletons. *Proc. Natl. Acad. Sci. USA* **2017**, *114*, E7670–E7678. [CrossRef]
97. Checa, A.G.; Macías-Sánchez, E.; Rodríguez-Navarro, A.B.; Sánchez-Navas, A.; Lagos, N.A. Origin of the biphase nature and surface roughness of biogenic calcite secreted by the giant barnacle *Austromegabalanus psittacus*. *Sci. Rep.* **2020**, *10*, 16784. [CrossRef]
98. Politi, Y.; Metzler, R.A.; Abrecht, M.; Gilbert, B.; Wilt, F.H.; Sagi, I.; Addadi, L.; Weiner, S.; Gilbert, P.U.P.A. Transformation mechanism of amorphous calcium carbonate into calcite in sea urchin larval spicule. *Proc. Natl. Acad. Sci. USA* **2008**, *105*, 17362–17366. [CrossRef] [PubMed]
99. Nash, M.C.; Diaz-Pulido, G.; Harvey, A.S.; Adey, W. Coralline algal calcification: A morphological and process-based understanding. *PLoS ONE* **2019**, *14*, e0221396. [CrossRef]
100. Jacob, D.E.; Wirth, R.; Agbaje, O.B.A.; Branson, O.; Eggins, S.M. Planktic foraminifera form their shells via metastable carbonate phases. *Nat. Commun.* **2017**, *8*, 1265. [CrossRef] [PubMed]
101. Comeau, S.; Cornwall, C.E.; DeCarlo, T.M.; Doo, S.S.; Carpenter, R.C.; McCulloch, M.T. Resistance to ocean acidification in coral reef taxa is not gained by acclimatization. *Nat. Clim. Chang.* **2019**, *9*, 477–483. [CrossRef]
102. Guillermic, M.; Cameron, L.P.; De Corte, I.; Misra, S.; Bijma, J.; De Beer, D.; Reymond, C.E.; Westphal, H.; Ries, J.B.; Robert, A.; et al. Thermal stress reduces pocilloporid coral resilience to ocean acidification by impairing control over calcifying fluid chemistry. *Sci. Adv.* **2021**, *7*, eaba9958. [CrossRef]
103. Soldati, A.L.; Jacob, D.; Glatzel, P.; Swarbrick, J.C.; Geck, J. Element substitution by living organisms: The case of manganese in mollusc shell aragonite. *Sci. Rep.* **2016**, *6*, 22514. [CrossRef] [PubMed]